DOI:
10.1016/j.sigpro.2018.08.015

Document Version
Peer reviewed version

An advanced beamforming approach based on two-channel echo-train system to cancel interference within an NQR signal resonance spectrum

Weihang Shao, Jamie Barras, Panagiotis Kosmas

PII: S0165-1684(18)30282-2
DOI: https://doi.org/10.1016/j.sigpro.2018.08.015
Reference: SIGPRO 6907

To appear in: *Signal Processing*

Received date: 6 May 2018
Revised date: 22 August 2018
Accepted date: 27 August 2018

Please cite this article as: Weihang Shao, Jamie Barras, Panagiotis Kosmas, An advanced beamforming approach based on two-channel echo-train system to cancel interference within an NQR signal resonance spectrum, *Signal Processing* (2018), doi: https://doi.org/10.1016/j.sigpro.2018.08.015

HIGHLIGHTS

- This paper introduces a two-channel echo-train (TE) data acquisition system used in NQR signal detection and discovers/proves the beamforming characteristics of the TE system.
- A novel beamforming approach based on this TE system is proposed which can nicely cancel interference within NQR resonance spectrum.
- The proposed algorithm has excellent performance on detecting NQR signal polluted by interference and is superior to previously proposed algorithms, including the classical beamforming algorithms/detectors constructed on the TE system.

An advanced beamforming approach based on two-channel echo-train system to cancel interference within an NQR signal resonance spectrum

Weihang Shao,[1] Jamie Barras,[1] and Panagiotis Kosmas[1]

[1]*Department of Informatics, King's College London*[*]

(Dated: August 29, 2018)

Abstract

Interference can be a huge challenge for Nuclear Quadrupole Resonance (NQR) signal detection in real life settings. The problem is particularly challenging when interference is strong around the resonant frequency band of the targeted NQR signal (to which we refer as the NQR band). This paper first proves the beamforming characteristics of a designed two-channel echo-train (TE) data acquisition system, and then presents a novel beamforming approach which is based on the TE system and is able to cancel interference effectively within the NQR band. After interference cancellation, NQR signal detection can be done successfully by applying an "echo train" approximate maximum likelihood (ETAML) algorithm to the residual data. The proposed algorithm is shown to be superior to previously proposed algorithms, including the classical beamforming algorithms/detectors constructed on the TE system, for detecting NQR signal polluted by interference.

[*] This work has been supported by Find a Better Way (FABW) UK, under Project AQUAREOS.

Emails:

weihang.shao@kcl.ac.uk (or picard314@hotmail.com),

jamie.barras@kcl.ac.uk,

panagiotis.kosmas@kcl.ac.uk.

I. INTRODUCTION

Electromagnetic (EM) waves can resonate quadrupolar nuclei which subsequently produce a response known as nuclear quadrupole resonance (NQR) signal [1]. The existence of materials or substances containing quadrupolar nuclei can be identified by detecting their featured NQR signals based on this principle. Applications of NQR signal detection include landmine detection, medicine authentication, security checking, oil drilling, etc, [2]. A typical quadrupolar nuclei that can be detected is ^{14}N, which is present in trinitrotoluen (TNT) in landmines and in the antimalarial medicine Metakelfin [3, 4].

NQR signals are well known for their very weak intensity and rapid attenuation. NQR data is collected with a spectrometer, which needs to fully relax before performing the next data collection. A mere spectrometer may lack efficiency because the relaxation stage may be quite long compared to the ”life period” of NQR signal, particularly for the detection of substances with long spin-lattice relaxation times, resulting in the waste of the remaining relaxation time after the NQR ”life period”. To overcome this limitation, an ”echo-train” technique based on pulsed spin locking sequences has been proposed [5, 6]. During a full relaxation time, the NQR signal can be echoed and recorded periodically by using this technique, and the intensity and initial phase of the NQR signal can be restored in every echo. Hence the whole system can record sufficiently long data within a full relaxation. Summing up all data echoes leads to a simple useful way to increase the signal to noise ratio (SNR), as the NQR signal can be added coherently as opposed to the stochastic noise which has random phase.

Unfortunately, data collection with this approach is prohibitively long in applications such as humanitarian demining and security checking, thereby preventing the acquisition of signals with sufficiently high SNRs for NQR detection. To overcome this problem, signal processing algorithms have been developed in recent years to achieve NQR detection in low SNR cases, for example [7, 8]. These algorithms identify the existence of the NQR signal using least squares or maximum likelihood theory to estimate NQR parameters which depend on the source substance, such as frequency, signal damping time, and echo decay time. The performance/robustness of related NQR detection algorithms has also been analyzed, as the noise has been well modeled and the Cramer-Rao Lower Bound has been discussed thoroughly [9]. In cases of extremely weak NQR signals, a novel approach based on stochastic resonance and neural network theory can also be applied to enhance detection [10]. This method in current stage, however, faces additional

challenges if strong interference is also present in the data.

In such situations of strong interference, Fourier-based spectrum analysis and frequency selective methods [8, 11] can deal successfully with interference that does not overlap significantly with the NQR signal's resonant frequency spectrum. In cases of strong overlaps, algorithms which include an interference cancellation (IC) step must be applied to improve NQR detection, as in our previous work in [12]. This algorithm, however, will inevitably affect the NQR signal if the interference is centred within the NQR band (i.e., the interval containing all possible values of the NQR signal resonant frequency under given environment conditions).

A different approach for cancelling interference can be based on using multiple channels for data collection. Researchers accordingly proposed useful (beamforming) algorithms for detecting NQR signals [13–17]. These algorithms can separate the NQR signal, the interference, and the noise assuming the three are non-correlated with each other, and select/detect the NQR signal. However, they have not provided a solution for dealing with interference which are highly correlated with the NQR signal. For canceling interference, one may consider a data acquisition system containing two channels: one to receive "primary" data which contains the NQR signal in the presence of background noise and interference, and the other to capture "secondary" data which only consists of the background noise and interference. In ideal conditions, interference can be cancelled perfectly by data subtraction from the two channels. In reality, however, calibration errors (such as "gain errors") and the different positions of the channels [13] result in amplitude and phase differences respectively between the data received from two channels, which prohibits direct subtraction. A pioneer two-channel NQR detection work which considers the calibration errors has been proposed recently [18]. Although this work theoretically proposes a good strategy for substracting interference, it highly relies on a precise measurement/knowledge on the gain error of the two channels, which is hard to satisfy in real-life settings. There is a similar work which also utilizes secondary channels for acquiring interference information [19]. This work, however, indirectly requires that the NQR signal subspace and the interference subspace should be orthogonal, which can not be satisfied when the frequencies of the NQR signal and the interference are the same or very close to each other. (For example, considering the continuous Hilbert space on $t \in [0, T]$, Subspace "$\cos(\frac{2\pi mt}{T} + \phi_1)$" and Subspace "$\cos(\frac{2\pi nt}{T} + \phi_2)$" is not orthogonal if $m = n$. Due to the same fact, we do not apply our IC method [12] inside the NQR band in case of cancelling the NQR signal.) Besides, this work also faces the problem of calibration errors. To this end, this paper proposes an advanced beamforming approach based on a two-channel echo-train

(TE) data acquisition system for interference cancellation within the NQR band. This approach first de-correlates the NQR signal and the interference utilizing the beamforming properties of the TE system. Then it precisely estimates the amplitude, frequency, and phase of the interference, which is robust to the calibration errors (gain errors). Combined with our previous IC technique [12], it can cancel interference in the whole frequency domain. Subsequently, the "echo-train" approximate maximum likelihood (ETAML) algorithm [8] can be applied to ensure a valid NQR detection strategy. The proposed algorithm is termed BICETAML (beamforming-based interference cancellation (BIC) + ETAML).

In the next section, we introduce the theory of the proposed BICETAML algorithm. In Section III, we apply the BICETAML algorithm to both simulated data and experimental data, and compare the results to those obtained by the previously proposed ETAML and FETAML algorithms as well as the classical beamforming detectors constructed on our TE system. The last section gives a summary of the main results.

II. THE THEORY OF THE BICETAML ALGORITHM

A. The data model

Recorded by a single-channel echo-train (SE) data acquisition system (see the upper row of Fig.1), a single-frequency NQR signal can be accurately modeled for the mth echo as [8]

$$y_m(t) = \alpha e^{-\frac{t+m\mu}{T^e}} e^{-\frac{|t-t_{sp}|}{T^*}+j2\pi\check{f}t}, \tag{1}$$

where t is the echo sampling time with the symmetric center to be t_{sp}, $2t_{sp}$ is called echo spacing, μ=$2t_{sp}$+μ' where μ' is the time gap between two neighbor echoes (μ' considered in this paper is 0 without loss of generality), and α, T^e, T^*, and $\check{f}$ are the amplitude, echo-train decay time, damping time, and frequency of the NQR signal, respectively. Any data z which contains the NQR signal can be divided into three parts: NQR signal y, noise n, and interference r, that is,

$$z_m(t) = y_m(t) + n_m(t) + r_m(t), \tag{2}$$

for the mth echo, where it is assumed that the noise n is white Gaussian and the interference r consists of several discrete single frequency components. If the sampling time for each echo is t=t_0, t_1 ..., t_{N-1} (unique sampling), and the total echo number is M in a practical measurement, the

entire data z can be rewritten in vector form as

$$\mathbf{Z}_{NM} = \mathbf{Y}_{NM} + \mathbf{N}_{NM} + \mathbf{R}_{NM}, \tag{3}$$

where $\mathbf{N}_{NM}$ and $\mathbf{R}_{NM}$ are the noise and interference parts, respectively. The signal part $\mathbf{Y}_{NM}$ satisfies

$$\mathbf{Y}_{NM} = \left[(y_1(\mathbf{t}))^{\mathrm{T}} \quad (y_2(\mathbf{t}))^{\mathrm{T}} \quad ... \quad (y_M(\mathbf{t}))^{\mathrm{T}}\right]^{\mathrm{T}} = \mathbf{Q}_{NM}\alpha, \tag{4}$$

where $\mathbf{t} = [t_0 \quad t_1 \quad ... \quad t_{N-1}]^{\mathrm{T}}$ is the time vector, $(.)^{\mathrm{T}}$ denotes the transpose, and $\mathbf{Q}_{NM}$ is the phase vector given by

$$\begin{aligned}\mathbf{Q}_{NM} &= \left[(\mathbf{Q}_m|_{m=1})^{\mathrm{T}} \quad (\mathbf{Q}_m|_{m=2})^{\mathrm{T}} \quad ... \quad (\mathbf{Q}_m|_{m=M})^{\mathrm{T}}\right]^{\mathrm{T}} \\ &= \left[e^{-\frac{(\mathbf{t}^{\mathrm{T}}+\mu)}{T^e}-\frac{|\mathbf{t}^{\mathrm{T}}-t_{sp}|}{T^*}+j2\pi\check{f}\mathbf{t}^{\mathrm{T}}} \quad e^{-\frac{(\mathbf{t}^{\mathrm{T}}+2\mu)}{T^e}-\frac{|\mathbf{t}^{\mathrm{T}}-t_{sp}|}{T^*}+j2\pi\check{f}\mathbf{t}^{\mathrm{T}}} \quad ... \right. \\ &\quad \left. e^{-\frac{(\mathbf{t}^{\mathrm{T}}+M\mu)}{T^e}-\frac{|\mathbf{t}^{\mathrm{T}}-t_{sp}|}{T^*}+j2\pi\check{f}\mathbf{t}^{\mathrm{T}}}\right]^{\mathrm{T}},\end{aligned} \tag{5}$$

respectively.

B. Review of the ETAML algorithm

If NQR signal components do exist in the received data, the values of signal parameters α, $\check{f}$, T^*, and T^e may be estimated based on maximum-likelihood theory, and the results should be close to the corresponding theoretical values. Based on this idea, the ETAML algorithm gives the estimation of signal amplitude α as

$$\hat{\alpha} = \mathbf{Q}_{NM}^{\dagger}\mathbf{Z}_{NM}, \tag{6}$$

where $(.)^{\dagger}$ denotes the Moore-Penrose pseudo-inverse. Accordingly, the likelihood function of $\check{f}$, T^*, and T^e is constructed as

$$L(\check{f}, T^*, T^e) = \mathbf{Z}_{NM}^{\mathrm{H}}\mathbf{Q}_{NM}\mathbf{Q}_{NM}^{\dagger}\mathbf{Z}_{NM}, \tag{7}$$

where $(.)^{\mathrm{H}}$ denotes the conjugate transpose. Then the estimated values of $\check{f}$, T^*, and T^e are obtained as

$$\left[\hat{\check{f}} \quad \hat{T}^* \quad \hat{T}^e\right] = \arg\max_{\check{f},T^*,T^e}(|L|). \tag{8}$$

The search ranges for $\check{f}$, T^*, and T^e should respectively cover all their possible values under immediate environment conditions based on knowledge of NQR theory [20]. In particular,

$$\check{f} = a - bTemp, \tag{9}$$

where $Temp$ is the environment temperature, and a and b are coefficients which are determined by the studied substance, respectively. If $Temp$ has an average value $Temp_0$ with an uncertainty ΔT, we have

$$\check{f} \in [a - bTemp_0 - b\Delta T, a - bTemp_0 + b\Delta T]. \tag{10}$$

We refer to Eq.(10) as the signal's NQR band, and use it as the search range for $\check{f}$ in this paper.

Once the estimated values $\hat{\check{f}}$, $\hat{T}^*$, and $\hat{T}^e$ are acquired, they can be substituted into the ETAML test statistic [21]

$$T(\mathbf{Z}_{NM}) = (2NM-1)\frac{\mathbf{Z}_{NM}^{\mathrm{H}}\mathbf{Q}_{NM}\mathbf{Q}_{NM}^{\dagger}\mathbf{Z}_{NM}}{\mathbf{Z}_{NM}^{\mathrm{H}}\mathbf{Z}_{NM} - \mathbf{Z}_{NM}^{\mathrm{H}}\mathbf{Q}_{NM}\mathbf{Q}_{NM}^{\dagger}\mathbf{Z}_{NM}}. \tag{11}$$

By predetermining a threshold value γ, the NQR signal is deemed present if and only if $T(\mathbf{Z}_{NM})>\gamma$, and otherwise not. An effective detection algorithm produces large $T(\mathbf{Z}_{NM})$ values when the NQR signal is present, and small ones otherwise, in order to give as few false alarms as possible.

Since the signal of interest is within the NQR band, applying ETAML algorithm only to frequency information within the NQR band should be enough and discards any interference outside (but without overlapping with) the NQR band [8, 12]. Selecting this frequency information can be done by dividing the NQR bands in a vector of J subbands $[f_{s1} \quad f_{s2} \quad ... \quad f_{sJ}]$ and then performing a DFT for $\mathbf{Z}_{NM}$ and $\mathbb{Q}_{NM}$ which yields

$$\begin{gathered}\left(\widetilde{\mathbf{Z}}_{JM}, \widetilde{\mathbb{Q}}_{JM}\right) = \begin{pmatrix} \mathbb{V}_J & & & \\ & \mathbb{V}_J & & \\ & & .. & \\ & & & \mathbb{V}_J \end{pmatrix} (\mathbf{Z}_{NM}, \mathbb{Q}_{NM}), \\ \mathbb{V}_J = \begin{pmatrix} 1 & e^{-j2\pi f_{s1}/f_s} & .. & e^{-j2\pi(N-1)f_{s1}/f_s} \\ 1 & e^{-j2\pi f_{s2}/f_s} & .. & e^{-j2\pi(N-1)f_{s2}/f_s} \\ .. & .. & .. & .. \\ 1 & e^{-j2\pi f_{sJ}/f_s} & .. & e^{-j2\pi(N-1)f_{sJ}/f_s} \end{pmatrix},\end{gathered} \tag{12}$$

where f_s is the sampling frequency. By combining this frequency selective method with ETAML, Eqs.(7) and (11) become,

$$\begin{aligned}\widetilde{L}(\omega_k, T_k^*, T_k^e) &= \widetilde{\mathbf{Z}}_{JM}^{\mathrm{H}}\widetilde{\mathbb{Q}}_{JM}\widetilde{\mathbb{Q}}_{JM}^{\dagger}\widetilde{\mathbf{Z}}_{JM}, \\ \widetilde{T}(\widetilde{\mathbf{Z}}_{JM}) &= (2JM-1)\frac{\widetilde{\mathbf{Z}}_{JM}^{\mathrm{H}}\widetilde{\mathbb{Q}}_{JM}\widetilde{\mathbb{Q}}_{JM}^{\dagger}\widetilde{\mathbf{Z}}_{JM}}{\widetilde{\mathbf{Z}}_{JM}^{\mathrm{H}}\widetilde{\mathbf{Z}}_{JM} - \widetilde{\mathbf{Z}}_{JM}^{\mathrm{H}}\widetilde{\mathbb{Q}}_{JM}\widetilde{\mathbb{Q}}_{JM}^{\dagger}\widetilde{\mathbf{Z}}_{JM}}.\end{aligned} \tag{13}$$

This combination is termed FETAML algorithm.

The ETAML algorithm is very useful for detecting NQR signals with low SNRs, but its performance degrades as interference increases. The FETAML algorithm, unfortunately, can only deal with some interference centered distant from the NQR band. For this reason, we have proposed an efficient IC method for cases with strong and even slightly time-varying interference overlapping with the NQR band [12]. This algorithm, however, do not deal with interference centered inside the (narrow) NQR band, which may occur in some real-life settings. This paper proposes an advanced beamforming-based interference cancellation (BIC) method based on a TE data acquisition system to tackle this type of interference. The entire TE system we build is illustrated in Fig.1.

C. The TE system and its beamforming characteristics

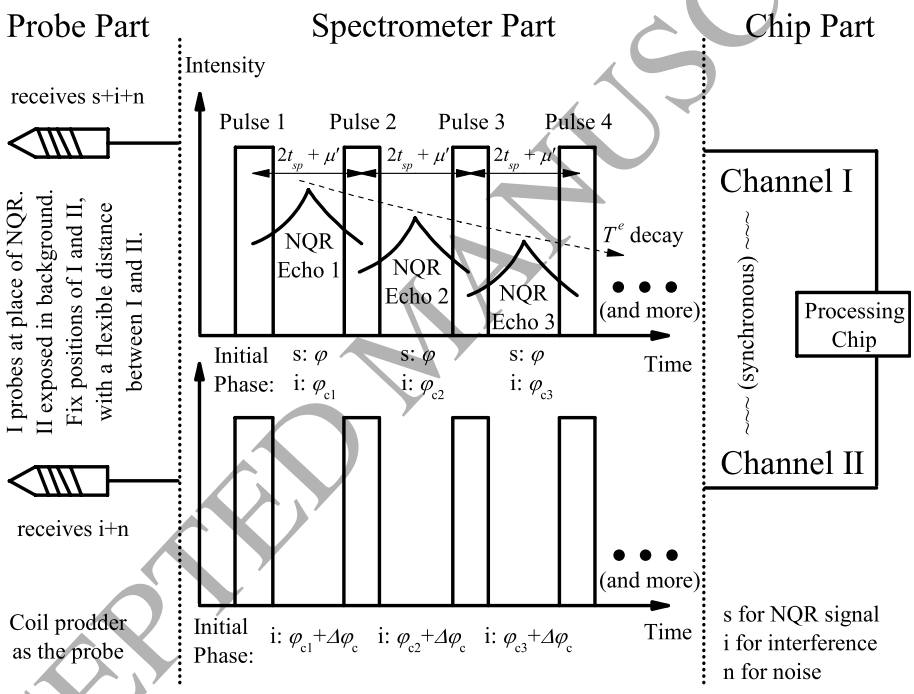

FIG. 1. (Color online) A sketch of the two-channel echo-train (TE) data acquisition system.

In this paper, we only consider that the interference present in the NQR band is single-frequency. In fact, the NQR band is usually very narrow thus likely "targeted" by single-frequency interference, and the possible sources of the strong interference are usually the electric appliances which are almost single-frequency. In particular, NQR signal is easily interfered by the spectrometer's pulse exciter which works at a frequency very close to NQR frequency and even within the NQR band. In addition, the interference considered here is stationary or slowly time-varying in-

terference, that is, its amplitude, frequency, and phase are constant or vary slightly with time. This is realistic in many practical applications where the spectrometer's full relaxation time is too short for interference to change its features significantly. Average calculations among the following related equations also strengthens the proposed algorithm's robustness to limited time-variation of interference.

In Fig.1, the upper row named Channel I consists of three parts indicating an entire work chain, from left to right, of a normal SE NQR data acquisition system. To realize a TE system, another work chain, the lower row named Channel II, is duplicated from and working synchronously with the Channel I, recording only the background noise and interference information (the so-called "secondary data") separately from the primary data received by the Channel I. The probe we use is a prodder with coil. The distance (array spacing) between the two probes can be flexible but should be fixed during data acquisition leading to a certain phase difference $\Delta\varphi_c$ ($\Delta\varphi_c \in [0, 2\pi)$) between the two channels' interference. The echo-train structure of the spectrometer only acts on NQR signal retrieving its initial phase at each pulse. Please see the NQR signal model, Eq.(1), where the initial phase (included in signal's complex amplitude α) is a constant for any echo. For interference, its initial phase at m-th echo, φ_{cm}, should be "$\mathrm{mod}\left[\varphi_{c1} + 2\pi f_c(2t_{sp} + \mu')(m-1), 2\pi\right]$" assuming interference is absolutely time-continuous, where f_c and φ_{c1} are interference's frequency and initial phase at 1-th echo, respectively. So, the initial phase of interference among echoes is quasi-random based on the facts that one can adjust t_{sp} and μ' to let $f_c(2t_{sp} + \mu')$ be non-integer and practically interference itself contains limited uncertainty.

Calibration error (gain error) between the two channels is inevitable producing small amplitude difference, also a bit of phase difference, between the two channels' received signals. The error may be different among different frequency components of received signals, and may even vary with time. The possible time-varying character of the calibration error, similar to that of interference, is limited within the short relaxation time of the spectrometer, and can be effectively tackled by the following average calculations.

The primary and secondary data vectors of the mth echo can be written as,

$$\begin{aligned}
\mathbf{Z}_m^{(\mathrm{p})} &= \left[Z_m^{(\mathrm{p})}(t_0) \quad Z_m^{(\mathrm{p})}(t_1) \quad \ldots \quad Z_m^{(\mathrm{p})}(t_{N-1})\right]^{\mathrm{T}} = \sigma_c e^{j2\pi f_c \mathbf{t} + j\varphi_{cm}} + \sigma(\mathbf{t}) \odot e^{j2\pi \check{f}\mathbf{t} + j\varphi} + \mathbf{N}_m^{(\mathrm{p})}, \\
\mathbf{Z}_m^{(\mathrm{s})} &= \left[Z_m^{(\mathrm{s})}(t_0) \quad Z_m^{(\mathrm{s})}(t_1) \quad \ldots \quad Z_m^{(\mathrm{s})}(t_{N-1})\right]^{\mathrm{T}} = (1+\epsilon)\sigma_c e^{j2\pi f_c \mathbf{t} + j\varphi_{cm} + j\Delta\varphi_c} + \mathbf{N}_m^{(\mathrm{s})},
\end{aligned} \tag{14}$$

where $\mathbf{N}_m^{(\mathrm{p})}$ and $\mathbf{N}_m^{(\mathrm{s})}$ denote the noise in the two channels, $\sigma(\mathbf{t})=|\alpha|e^{-\frac{\mathbf{t}+m\mu}{T^e} - \frac{|\mathbf{t}-t_{sp}|}{T^*}}$ (practically, $T^e \gg T^*$, which means that $\sigma(\mathbf{t}) \simeq |\alpha| e^{-\frac{|\mathbf{t}-t_{sp}|}{T^*}}$), φ denotes the received NQR signal's initial phase which in fact

is the argument of α ($\alpha = |\alpha|e^{j\varphi}$), f_c ($f_c \simeq \check{f}$) is the frequency of interference, σ_c is the amplitude of interference in primary channel, and "$\odot$" denotes the element by element multiplication, respectively. In Eq.(14), ϵ is introduced to account for the calibration error on amplitude difference between the two channels for the single-frequency interference with the NQR band. Our analysis considers a range of values $-0.5 \le \epsilon \le 1$ which should cover most practical situations. As is mentioned, ϵ as well as the phase difference $\Delta\varphi_c$ of interference can also be time-varying with limited fluctuations, in which case we may simply take their averages into the following derivations. In fact, as shown in Eqs.(39) and (41), the estimation on large interference amplitude is robust to the variation of ϵ and $\Delta\varphi_c$.

According to beamforming theory, the so called "steering vectors" of the m-th echo NQR signal and interference are respectively

$$\begin{aligned} \mathbf{a}_m(t) &= \left[e^{j2\pi\check{f}t+j\varphi} \quad 0\right]^{\mathrm{T}}, \\ \mathbf{a}_{cm}(t) &= \left[e^{j2\pi f_c t+j\varphi_{cm}} \quad (1+\epsilon)e^{j2\pi f_c t+j\varphi_{cm}+j\Delta\varphi_c}\right]^{\mathrm{T}}. \end{aligned} \tag{15}$$

Furthermore, the beamforming covariance matrix of the m-th echo is obtained as "$\overline{\mathbb{R}_m}=\frac{1}{N}\sum_{i=0}^{N-1}\mathbb{R}_m|_{t_i}$", where

$$\begin{aligned} \mathbb{R}_m|_t &= \left[Z_m^{(\mathrm{p})}(t) \quad Z_m^{(\mathrm{s})}(t)\right]^{\mathrm{T}}\left\{\left[Z_m^{(\mathrm{p})}(t) \quad Z_m^{(\mathrm{s})}(t)\right]^{\mathrm{T}}\right\}^{\mathrm{H}} \\ &= \sigma(t)\sigma_c\left[\mathbf{a}_m(t)\mathbf{a}_{cm}^{\mathrm{H}}(t)+\mathbf{a}_{cm}(t)\mathbf{a}_m^{\mathrm{H}}(t)\right] \\ &\quad +\sigma^2(t)\mathbf{a}_m(t)\mathbf{a}_m^{\mathrm{H}}(t)+\sigma_c^2\mathbf{a}_{cm}(t)\mathbf{a}_{cm}^{\mathrm{H}}(t)+\mathbb{R}_{\mathrm{cc}}, \end{aligned} \tag{16}$$

is a 2×2 matrix with its 4 elements being,

$$\begin{aligned} \mathbb{R}_m(1,1) &= 2\sigma(t)\sigma_c\cos\left[(2\pi\check{f}t+\varphi)-(2\pi f_c t+\varphi_{cm})\right] \\ &\quad +\sigma^2(t)+\sigma_c^2+\mathbb{R}_{\mathrm{cc}}(1,1), \\ \mathbb{R}_m(1,2) &= \sigma(t)\sigma_c(1+\epsilon)e^{j(2\pi\check{f}t+\varphi)-j(2\pi f_c t+\varphi_{cm}+\Delta\varphi_c)} \\ &\quad +\sigma_c^2(1+\epsilon)e^{-j\Delta\varphi_c}+\mathbb{R}_{\mathrm{cc}}(1,2), \\ \mathbb{R}_m(2,1) &= \sigma(t)\sigma_c(1+\epsilon)e^{j(2\pi f_c t+\varphi_{cm}+\Delta\varphi_c)-j(2\pi\check{f}t+\varphi)} \\ &\quad +\sigma_c^2(1+\epsilon)e^{j\Delta\varphi_c}+\mathbb{R}_{\mathrm{cc}}(2,1), \\ \mathbb{R}_m(2,2) &= (1+\epsilon)^2\sigma_c^2+\mathbb{R}_{\mathrm{cc}}(2,2), \end{aligned} \tag{17}$$

where $\overline{\mathbb{R}_{\mathrm{cc}}}$ is the autocorrelation of the noise satisfying $\overline{\mathbb{R}_{\mathrm{cc}}}(1,1) = \sigma_{N\mathrm{p}}^2$ and $\overline{\mathbb{R}_{\mathrm{cc}}}(2,2) = \sigma_{N\mathrm{s}}^2$, $\sigma_{N\mathrm{p}}^2$ and $\sigma_{N\mathrm{s}}^2$ are the variances of noise respectively in the primary and secondary channels, and

$\overline{\mathbb{R}_{\rm cc}}(1,2) = \overline{\mathbb{R}_{\rm cc}}(2,1) = 0$ since noise and interference (or NQR signal) are incoherent. By averaging over echoes "$\overline{\overline{\mathbb{R}}}=\frac{1}{M}\sum_{m=1}^{M}\overline{\mathbb{R}_m}$", for large enough M, we can eliminate the coherence between the NQR signal and the interference, since that φ_{cm} is as mentioned before a quasi-random variable which leads to

$$\begin{aligned}
&\frac{1}{M}\sum_{m=1}^{M} 2\sigma(t)\sigma_c \cos\left[(2\pi\check{f}t+\varphi)-(2\pi f_c t+\varphi_{cm})\right] \to 0,\\
&\frac{1}{M}\sum_{m=1}^{M} \sigma(t)\sigma_c(1+\epsilon)e^{j(2\pi\check{f}t+\varphi)-j(2\pi f_c t+\varphi_{cm}+\Delta\varphi_c)} \to 0,\\
&\frac{1}{M}\sum_{m=1}^{M} \sigma(t)\sigma_c(1+\epsilon)e^{j(2\pi f_c t+\varphi_{cm}+\Delta\varphi_c)-j(2\pi\check{f}t+\varphi)} \to 0.
\end{aligned} \tag{18}$$

We then obtain

$$\begin{aligned}
\overline{\overline{\mathbb{R}}} &\simeq \begin{pmatrix} \overline{\sigma^2(t)}+\sigma_c^2+\sigma_{N\rm p}^2 & \sigma_c^2(1+\epsilon)e^{-j\Delta\varphi_c} \\ \sigma_c^2(1+\epsilon)e^{j\Delta\varphi_c} & (1+\epsilon)^2\sigma_c^2+\sigma_{N\rm s}^2 \end{pmatrix}\\
&= \sigma_c^2\mathbf{a}_c\mathbf{a}_c^{\rm H} + \begin{pmatrix} \overline{\sigma^2(t)}+\sigma_{N\rm p}^2 & 0 \\ 0 & \sigma_{N\rm s}^2 \end{pmatrix},
\end{aligned} \tag{19}$$

where $\mathbf{a}_c = \begin{bmatrix}1 & (1+\epsilon)e^{j\Delta\varphi_c}\end{bmatrix}^{\rm T}$. The beamforming characteristics of the TE system is proven as the derived Eq.(19) is well-known in beamforming theory [22].

D. Constructing classical beamforming detectors

We first consider constructing the classical beamforming detectors (BFDs), the Capon and the maximum likelihood (ML) [17], based on the TE data acquisition system.

For decorrelating interference and NQR signal, we have to average the beamforming covariance matrix $\overline{\mathbb{R}_m}$ (see Eq.(18)), which prohibits the direct implementation of the Capon BFD. However, following the Capon BFD theory and using the NQR signal steering vector $\mathbf{a}_m(t)$ in Eq.(15), we can write the Capon beamforming output BO_s for the NQR signal as,

$$\begin{aligned}
\mathrm{BO}_s &= \frac{1}{\mathbf{a}_m^{\rm H}\left(\overline{\overline{\mathbb{R}}}\right)^{-1}\mathbf{a}_m} = \frac{1}{\mathbf{a}_1^{\rm H}\left(\overline{\overline{\mathbb{R}}}\right)^{-1}\mathbf{a}_1}\\
&\simeq \overline{\sigma^2(t)}+\sigma_{N\rm p}^2 + \frac{\sigma_c^2\sigma_{N\rm s}^2}{(1+\epsilon)^2\sigma_c^2+\sigma_{N\rm s}^2},
\end{aligned} \tag{20}$$

where $\mathbf{a}_1=[1 \quad 0]^{\mathrm{T}}$. Apparently, BO_s can be served as a beamforming detector as it does not contain the first term $\overline{\sigma^2(t)}$ when there is no NQR signal. Similar to utilizing Eq.(11), we can predetermine a threshold value γ. The NQR signal is deemed present if and only if $\mathrm{BO}_s>\gamma$, and otherwise not.

Following the ML BFD theory [22], we can accordingly write the estimation of NQR signal's amplitude, $\hat{\alpha}$, as

$$\begin{aligned}\hat{\alpha} &= \arg\min_{\alpha}\left|\frac{1}{NM}\sum_{m=1}^{M}\sum_{n=0}^{N-1}\left(\mathbf{x}_{nm}-\mathbf{a}_1\alpha s_{nm}\right)\left(\mathbf{x}_{nm}-\mathbf{a}_1\alpha s_{nm}\right)^{\mathrm{H}}\right| \\ &= \arg\min_{\alpha}\left|\overline{\overline{\mathbb{R}}}-\bar{\mathbf{x}}\left(\mathbf{a}_1\alpha\right)^{\mathrm{H}}-\left(\mathbf{a}_1\alpha\right)\bar{\mathbf{x}}^{\mathrm{H}}+\left(\mathbf{a}_1\alpha\right)P_s\left(\mathbf{a}_1\alpha\right)^{\mathrm{H}}\right| \\ &\triangleq \arg\min_{\alpha}\left|\mathbb{Q}_{\mathrm{MLBFD}}\right|,\end{aligned} \tag{21}$$

where $\mathbf{x}_{nm}=\left[Z_m^{(\mathrm{p})}(t_n) \quad Z_m^{(\mathrm{s})}(t_n)\right]^{\mathrm{T}}$ is the so-called data snapshots, $s_{nm}=e^{j2\pi\check{f}t_{\neg}-\frac{|t_n+m\mu|}{T^e}-\frac{|t_n-t_{sp}|}{T^*}}$ is the NQR waveform, and $\triangleq$ means "defined as", respectively. We can derive that,

$$\hat{\alpha}=\frac{\mathbf{a}_1^{\mathrm{H}}\mathbb{T}^{-1}\bar{\mathbf{x}}}{P_s\mathbf{a}_1^{\mathrm{H}}\mathbb{T}^{-1}\mathbf{a}_1}, \tag{22}$$

where

$$\bar{\mathbf{x}}=\frac{1}{NM}\sum_{m=1}^{M}\sum_{n=0}^{N-1}\mathbf{x}_{nm}s_{nm}^{*}, \tag{23}$$

and

$$P_s=\frac{1}{NM}\sum_{m=1}^{M}\sum_{n=0}^{N-1}s_{nm}s_{nm}^{*}, \tag{24}$$

and

$$\mathbb{T}=\overline{\overline{\mathbb{R}}}-\frac{\bar{\mathbf{x}}\bar{\mathbf{x}}^{\mathrm{H}}}{P_s}, \tag{25}$$

respectively. Substituting Eq.(22) into Eq.(21) leads to the estimation of the NQR parameters $\left[\check{f} \quad T^* \quad T^e\right]$ [16],

$$\left[\hat{\check{f}} \quad \hat{T}^* \quad \hat{T}^e\right]=\arg\min_{\check{f},T^*,T^e}\left|\mathbb{Q}_{\mathrm{MLBFD}}\left(\hat{\alpha}\right)\right|. \tag{26}$$

The test statistic T_{MLBFD} of the ML BFD can be written as [16],

$$T_{\mathrm{MLBFD}}=NM\left(\ln\left|\overline{\overline{\mathbb{R}}}\right|-\ln\left|\mathbb{Q}_{\mathrm{MLBFD}}\left(\hat{\alpha}\right)|_{\hat{\check{f}},\hat{T}^*,\hat{T}^e}\right|\right), \tag{27}$$

Similar to utilizing Eq.(11), we can predetermine a threshold value γ. The NQR signal is deemed present if and only if $T_{\mathrm{MLBFD}}>\gamma$, and otherwise not.

Similar to acquiring Eq.(18), we can derive $\bar{\mathbf{x}}\rightarrow[\alpha P_s \quad 0]^{\mathrm{T}}$ for large enough M. Then, since that $\bar{\mathbf{x}}(1)^{\mathrm{H}}\bar{\mathbf{x}}(1)/P_s=(\alpha P_s)^{\mathrm{H}}(\alpha P_s)/P_s=\overline{\sigma^2(t)}$, we have

$$\mathbb{T} \simeq \begin{pmatrix} \sigma_c^2+\sigma_{N\mathrm{p}}^2 & \sigma_c^2(1+\epsilon)e^{-j\Delta\varphi_c} \\ \sigma_c^2(1+\epsilon)e^{j\Delta\varphi_c} & (1+\epsilon)^2\sigma_c^2+\sigma_{N\mathrm{s}}^2 \end{pmatrix}, \tag{28}$$

$\hat{\alpha}\rightarrow\alpha$ which means that Eq.(22) gives an unbiased estimation of α, and $\bar{\mathbf{x}}(1)^{\mathrm{H}}\bar{\mathbf{x}}(1)$ may also be considered as an NQR detector. However, it is noted that there is little difference between $\bar{\mathbf{x}}(1)^{\mathrm{H}}\bar{\mathbf{x}}(1)$ and the likelihood function (see Eq.(7)) of the ETAML algorithm, as we can derive,

$$\mathbf{Q}_{NM}^{\dagger} = \frac{\mathbf{Q}_{NM}^{\mathrm{H}}}{\mathbf{Q}_{NM}^{\mathrm{H}}\mathbf{Q}_{NM}}. \tag{29}$$

So,

$$\mathbf{Q}_{NM}^{\dagger}\mathbf{Z}_{NM} = \frac{\bar{\mathbf{x}}(1)}{\mathbf{Q}_{NM}^{\mathrm{H}}\mathbf{Q}_{NM}}. \tag{30}$$

Since that the value of $1/\mathbf{Q}_{NM}^{\mathrm{H}}\mathbf{Q}_{NM}$ with different $\check{f}$, T^*, and T^e can be approximately regarded as a constant, we approximately have

$$\bar{\mathbf{x}}(1)^{\mathrm{H}}\bar{\mathbf{x}}(1) \propto \left(\mathbf{Q}_{NM}^{\dagger}\mathbf{Z}_{NM}\right)^{\mathrm{H}}\mathbf{Q}_{NM}^{\dagger}\mathbf{Z}_{NM} \propto \mathbf{Z}_{NM}^{\mathrm{H}}\mathbf{Q}_{NM}\mathbf{Q}_{NM}^{\dagger}\mathbf{Z}_{NM}, \tag{31}$$

which implies that $\bar{\mathbf{x}}(1)^{\mathrm{H}}\bar{\mathbf{x}}(1)$ and ETAML are approximately equivalent.

Like ETAML, the ML BFD can also be coupled with the frequency-selective method mentioned before [16]. Referring to Eq.(12), we have

$$\begin{aligned}
&\widetilde{\mathbf{Z}}_m^{(\mathrm{o})} = \mathbb{V}_J\mathbf{Z}_m^{(\mathrm{o})}, \quad \text{"o"} = \text{"p" or "s"},\\
&\widetilde{\mathbf{x}}_{jm} = \left[\widetilde{\mathbf{Z}}_m^{(\mathrm{o})}(j) \quad \widetilde{\mathbf{Z}}_m^{(\mathrm{s})}(j)\right]^{\mathrm{T}}, \quad \widetilde{\mathbf{Q}}_m = \mathbb{V}_J\mathbf{Q}_m, \quad \widetilde{s}_{jm} = \widetilde{\mathbf{Q}}_m(j),\\
&\widetilde{\widetilde{\mathbb{R}}} = \frac{1}{JM}\sum_{m=1}^{M}\sum_{j=1}^{J}\widetilde{\mathbf{x}}_{jm}\widetilde{\mathbf{x}}_{jm}^{\mathrm{H}}, \quad \widetilde{\bar{\mathbf{x}}} = \frac{1}{JM}\sum_{m=1}^{M}\sum_{j=1}^{J}\widetilde{\mathbf{x}}_{jm}\widetilde{s}_{jm}^{*},\\
&\widetilde{P}_s = \frac{1}{JM}\sum_{m=1}^{M}\sum_{j=1}^{J}\widetilde{s}_{jm}\widetilde{s}_{jm}^{*}, \quad \widetilde{\mathbb{T}} = \widetilde{\widetilde{\mathbb{R}}} - \frac{\widetilde{\bar{\mathbf{x}}}\widetilde{\bar{\mathbf{x}}}^{\mathrm{H}}}{\widetilde{P}_s},\\
&\widetilde{\mathbb{Q}}_{\mathrm{MLBFD}} = \widetilde{\widetilde{\mathbb{R}}} - \widetilde{\bar{\mathbf{x}}}(\mathbf{a}_1\alpha)^{\mathrm{H}} - (\mathbf{a}_1\alpha)\widetilde{\bar{\mathbf{x}}}^{\mathrm{H}} + (\mathbf{a}_1\alpha)\widetilde{P}_s(\mathbf{a}_1\alpha)^{\mathrm{H}}.
\end{aligned} \tag{32}$$

The frequency-selective ML BFD is implemented as,

$$\begin{aligned}
&\hat{\alpha} = \frac{\mathbf{a}_1^{\mathrm{H}}\widetilde{\mathbb{T}}^{-1}\widetilde{\bar{\mathbf{x}}}}{\widetilde{P}_s\mathbf{a}_1^{\mathrm{H}}\widetilde{\mathbb{T}}^{-1}\mathbf{a}_1},\\
&\left[\hat{\check{f}} \quad \hat{T}^* \quad \hat{T}^e\right] = \arg\min_{\check{f},T^*,T^e}\left|\widetilde{\mathbb{Q}}_{\mathrm{MLBFD}}(\hat{\alpha})\right|,\\
&\widetilde{T}_{\mathrm{MLBFD}} = JM\left(\ln\left|\widetilde{\widetilde{\mathbb{R}}}\right| - \ln\left|\widetilde{\mathbb{Q}}_{\mathrm{MLBFD}}(\hat{\alpha})\Big|_{\hat{\check{f}},\hat{T}^*,\hat{T}^e}\right|\right).
\end{aligned} \tag{33}$$

Although the classical ML BFD does not consider decorrelating signal and interference whose frequencies are very close to each other, we find that under the current TE data acquisition system, the related derivation coincidentally yields $\overline{\overline{\mathbb{R}}}$ and $\bar{\mathbf{x}}$ where NQR signal and interference are decorrelated.

E. The BIC method

The previous subsection presents how we implement the classical beamforming methods on our TE system. These methods indeed indirectly cancel the interference but they may not outperform our proposed BIC method introduced in the following. There are detailed performance comparisons as well as the related analysis in Section III.

The BIC method first estimates the interference's amplitude σ_c. We introduce the weight vector $\mathbf{w}$ and beamforming output BO=$\mathbf{w}^{\mathrm{H}}\overline{\overline{\mathbb{R}}}\mathbf{w}$ for the interference [13], where $\mathbf{w}$ is the solution of the

$$\min_{\mathbf{w}} \mathbf{w}^{\mathrm{H}}\overline{\overline{\mathbb{R}}}\mathbf{w} \quad \text{subject to } \mathbf{w}^{\mathrm{H}}\mathbf{a}_c = 1. \tag{34}$$

Using Lagrange's multiplier method or a Cauchy inequality, one can obtain

$$\mathbf{w} = \frac{\left(\overline{\overline{\mathbb{R}}}\right)^{-1}\mathbf{a}_c}{\mathbf{a}_c^{\mathrm{H}}\left(\overline{\overline{\mathbb{R}}}\right)^{-1}\mathbf{a}_c}, \tag{35}$$

where $\left(\overline{\overline{\mathbb{R}}}\right)^{-1}$ is the inverse of $\overline{\overline{\mathbb{R}}}$ and satisfies

$$\left(\overline{\overline{\mathbb{R}}}\right)^{-1} \simeq \frac{\begin{pmatrix} (1+\epsilon)^2\sigma_c^2 + \sigma_{N\mathrm{s}}^2 & -\sigma_c^2(1+\epsilon)e^{-j\Delta\varphi_c} \\ -\sigma_c^2(1+\epsilon)e^{j\Delta\varphi_c} & \overline{\sigma^2(t)} + \sigma_c^2 + \sigma_{N\mathrm{p}}^2 \end{pmatrix}}{\left(\overline{\sigma^2(t)} + \sigma_{N\mathrm{p}}^2\right)\left[(1+\epsilon)^2\sigma_c^2 + \sigma_{N\mathrm{s}}^2\right] + \sigma_c^2\sigma_{N\mathrm{s}}^2}. \tag{36}$$

The beamforming output BO for the interference can be rewritten as,

$$\mathrm{BO} = \min_{\mathbf{w}} \mathbf{w}^{\mathrm{H}}\overline{\overline{\mathbb{R}}}\mathbf{w} \simeq \sigma_c^2 + \min_{\mathbf{w}} \mathbf{w}^{\mathrm{H}}\left(\overline{\overline{\mathbb{R}}} - \mathbb{C}\right)\mathbf{w}, \tag{37}$$

where $\mathbb{C} = \sigma_c^2\mathbf{a}_c\mathbf{a}_c^{\mathrm{H}}$ and BO can be the estimation of σ_c^2 if $\min_{\mathbf{w}} \mathbf{w}^{\mathrm{H}}\left(\overline{\overline{\mathbb{R}}} - \mathbb{C}\right)\mathbf{w}$ is small enough. Substituting Eq.(35) into Eq.(37) yields,

$$\begin{aligned} \mathrm{BO} = \mathbf{w}^{\mathrm{H}}\overline{\overline{\mathbb{R}}}\mathbf{w} &= \frac{1}{\mathbf{a}_c^{\mathrm{H}}\left(\overline{\overline{\mathbb{R}}}\right)^{-1}\mathbf{a}_c} \\ &\simeq \sigma_c^2 + \frac{\sigma_{N\mathrm{s}}^2\left(\overline{\sigma^2(t)} + \sigma_{N\mathrm{p}}^2\right)}{\sigma_{N\mathrm{s}}^2 + \left(\overline{\sigma^2(t)} + \sigma_{N\mathrm{p}}^2\right)(1+\epsilon)^2}. \end{aligned} \tag{38}$$

This means that,

$$\sigma_c^2 \leq \mathrm{BO} \leq \sigma_c^2 + \min\left\{\frac{\sigma_{N\mathrm{s}}^2}{(1+\epsilon)^2}, \left(\overline{\sigma^2(t)} + \sigma_{N\mathrm{p}}^2\right)\right\}. \tag{39}$$

Thus, $\mathrm{BO} \simeq \sigma_c^2$ in the case of strong interference.

Please note that Eqs.(34)-(39) take the exact ϵ and $\Delta\varphi_c$ which, however, are unknown in our TE settings, *i.e.*, $\mathbf{a}_c$ is unknown. However, inspired by Eq.(39), we introduce two variables ϵ_x and Δ_y, and their functions $\mathbf{a}_{cf} = \begin{bmatrix}1 & (1+\epsilon_x)e^{j\Delta_y}\end{bmatrix}^{\mathrm{T}}$ and

$$\mathrm{BO}_f = \frac{1}{\mathbf{a}_{cf}^{\mathrm{H}}\left(\overline{\overline{\mathbb{R}}}\right)^{-1}\mathbf{a}_{cf}}, \tag{40}$$

corresponding to ϵ, $\Delta\varphi_c$, $\mathbf{a}_c$, and BO. BO_f=BO when ϵ_x=ϵ and Δ_y=$\Delta\varphi_c$. Substituting Eq.(36) into Eq.(40) yields

$$\mathrm{BO}_f \simeq \frac{\left(\overline{\sigma^2(t)} + \sigma_{N\mathrm{p}}^2\right)\left[(1+\epsilon)^2\sigma_c^2 + \sigma_{N\mathrm{s}}^2\right] + \sigma_c^2\sigma_{N\mathrm{s}}^2}{\left(\overline{\sigma^2(t)} + \sigma_c^2 + \sigma_{N\mathrm{p}}^2\right)\left[(1+\epsilon_x) - \frac{(1+\epsilon)\sigma_c^2\cos\left(\Delta_y-\Delta\varphi_c\right)}{\overline{\sigma^2(t)}+\sigma_c^2+\sigma_{N\mathrm{p}}^2}\right]^2 + (1+\epsilon)^2\sigma_c^2 + \sigma_{N\mathrm{s}}^2 - \frac{(1+\epsilon)^2\sigma_c^4\cos^2\left(\Delta_y-\Delta\varphi_c\right)}{\overline{\sigma^2(t)}+\sigma_c^2+\sigma_{N\mathrm{p}}^2}}. \tag{41}$$

Apparently, BO_f reaches its maximum, $\max\left(\mathrm{BO}_f\right) \simeq \overline{\sigma^2(t)}+\sigma_c^2+\sigma_{N\mathrm{p}}^2$, when Δ_y=$\Delta\varphi_c$ and ϵ_x=$\frac{(1+\epsilon)\sigma_c^2}{\overline{\sigma^2(t)}+\sigma_c^2+\sigma_{N\mathrm{p}}^2}$ − 1. It is noted that $\max\left(\mathrm{BO}_f\right) \simeq \sigma_c^2$ and $\epsilon_x \simeq \epsilon$ for strong interference cases, and we issue the specific beamforming problem for our TE system as

$$\hat{\sigma}_c = \sqrt{\max_{\epsilon_x,\Delta_y} \mathrm{BO}_f}, \tag{42}$$

which is the estimation of σ_c, where the ranges of ϵ_x and Δ_y are $[-0.5, 1]$ and $[0, 2\pi)$, respectively, as mentioned before. It is worth noting that one may also think about using robust Capon Beamforming (RCB) [13] method to estimate the interference amplitude σ_c. However, RCB theoretically demands a prior knowledge (with limited uncertainty) of ϵ and $\Delta\varphi_c$, and the comparison between the proposed method and RCB shows that RCB method is not suitable for solving the present problem. Please see the Appendix for more information.

After $\hat{\sigma}_c$ is obtained, we must also estimate the exact frequency and initial phase of the interference in order to cancel it from the original NQR data (only in the primary channel). Given that the frequency component of each echo of secondary data with the strongest intensity should correspond to interference's frequency, we can estimate the interference's frequency f_c as the least-square solution,

$$\min_f \left\| \mathbf{Z}_m^{(\mathrm{s})} - e^{j2\pi f\mathbf{t}}\left(e^{j2\pi f\mathbf{t}}\right)^{\dagger}\mathbf{Z}_m^{(\mathrm{s})} \right\|_2^2, \quad f \in \text{NQR band}, \tag{43}$$

where $\left(e^{j2\pi f\mathbf{t}}\right)^{\dagger}\mathbf{Z}_m^{(\mathrm{s})}$ is the amplitude estimation of frequency component of f. Once we have $\hat{f}_c$, we can estimate the initial phase φ_{cm}. By setting $\phi_m = e^{j\varphi_{cm}}$ as the phase factor of the interference in the m-th echo and using again the least-square method, the phase estimation $\hat{\phi}_m$ is the solution of,

$$\min_{\phi_m}\left\|\mathbf{Z}_m^{(\mathrm{p})} - \hat{\sigma}_c e^{j2\pi\hat{f}_c\mathbf{t}}\phi_m\right\|_2^2 \quad \text{subject to } |\phi_m| = 1, \tag{44}$$

for the m-th echo. φ_{cm} can of course be calculated numerically within the searching range $[0, 2\pi)$. However, we derive a way to calculate φ_{cm} analytically for saving calculation cost. In fact, $\left\|\mathbf{Z}_m^{(\mathrm{p})} - \hat{\sigma}_c e^{j2\pi\hat{f}_c\mathbf{t}}\phi_m\right\|_2^2$ as a function of φ_{cm} is a polynomial of trigonometric function of φ_{cm}. It should have two extremums for $\varphi_{cm} \in [0, 2\pi)$. To find them, we construct the Lagrange function,

$$\begin{aligned} L_m(\phi_m) = &\left(\mathbf{Z}_m^{(\mathrm{p})} - \hat{\sigma}_c e^{j2\pi\hat{f}_c\mathbf{t}}\phi_m\right)^{\mathrm{H}}\left(\mathbf{Z}_m^{(\mathrm{p})} - \hat{\sigma}_c e^{j2\pi\hat{f}_c\mathbf{t}}\phi_m\right) \\ &+ \lambda\left(\phi_m^*\phi_m - 1\right), \end{aligned} \tag{45}$$

where (.)* denotes the conjugation and λ is the Lagrange multiplier. Setting $\frac{\partial L_m}{\partial \phi_m} = 0$ yields

$$\left[-\left(\mathbf{Z}_m^{(\mathrm{p})}\right)^{\mathrm{H}}\hat{\sigma}_c e^{j2\pi\hat{f}_c\mathbf{t}} + \phi_m^*\hat{\sigma}_c^2 + \lambda\phi_m^*\right]\left(\frac{\mathrm{d}\phi_m^*}{\mathrm{d}\phi_m} + 1\right) = 0, \tag{46}$$

that is,

$$\hat{\phi}_m = \frac{\hat{\sigma}_c e^{-j2\pi\hat{f}_c\mathbf{t}^{\mathrm{T}}}\mathbf{Z}_m^{(\mathrm{p})}}{\left(\hat{\sigma}_c^2 + \lambda\right)^*}. \tag{47}$$

Similarly, $\frac{\partial L_m}{\partial \lambda} = 0$ (or $|\phi_m| = 1$) yields

$$\left(\hat{\sigma}_c^2 + \lambda\right)^*\left(\hat{\sigma}_c^2 + \lambda\right) = \hat{\sigma}_c^2\left(\mathbf{Z}_m^{(\mathrm{p})}\right)^{\mathrm{H}} e^{j2\pi\hat{f}_c\mathbf{t}}e^{-j2\pi\hat{f}_c\mathbf{t}^{\mathrm{T}}}\mathbf{Z}_m^{(\mathrm{p})}. \tag{48}$$

Letting λ be a real number, we have

$$\hat{\phi}_{m\pm} = \pm\frac{e^{-j2\pi\hat{f}_c\mathbf{t}^{\mathrm{T}}}\mathbf{Z}_m^{(\mathrm{p})}}{\sqrt{\left(\mathbf{Z}_m^{(\mathrm{p})}\right)^{\mathrm{H}} e^{j2\pi\hat{f}_c\mathbf{t}}e^{-j2\pi\hat{f}_c\mathbf{t}^{\mathrm{T}}}\mathbf{Z}_m^{(\mathrm{p})}}}, \tag{49}$$

which corresponds to the two extremums. The solution is of course the minimum one, that is,

$$\hat{\phi}_m = \min\left(L_m\left(\hat{\phi}_{m+}\right), L_m\left(\hat{\phi}_{m-}\right)\right). \tag{50}$$

Thus, the interference cancelled data of the m-th echo is $\mathbf{Z}_m^{(\mathrm{p})} - \hat{\sigma}_c e^{j2\pi\hat{f}_c\mathbf{t}}\hat{\phi}_m$, which can then be processed by the ETAML algorithm to detect accurately the NQR signal.

F. Combining the BIC with the previous IC method to suppress interference across the whole data spectrum

The presented BIC approach was designed to focus on interference that occurs predominantly inside the NQR band. However, before applying the BIC approach, we must apply our recently proposed IC method [12] to remove possibly existing interference outside the NQR band. This section reviews the methodology developed in [12] for this purpose, and also discusses how this approach can be applied as an IC step prior to the BIC method without compromising its performance.

To apply the IC method outside the NQR band, we discretize the frequency interval "$\left[-\frac{f_s}{2}, \frac{f_s}{2}\right]$-NQR band", where f_s=1/ $(t_1 - t_0)$ is the sampling frequency, to a vector of frequencies $[f_1, f_2, ..., f_K]$. Using the Fourier vectors $\mathbf{F}(f_k) = e^{j2\pi f_k \mathbf{t}}$, $k = 1, 2, ..., K$, interference outside the NQR band can be cancelled following the steps in Table 1 [12]. Assuming stationary or slowly time-varying interference (as also mentioned before), the algorithm in Table 1 models interference using a linear combination of Fourier basis functions, and estimates at each iteration interference's most significant frequency component, f_{mi}, $i = 1, 2, ...$, using the cost function C. The component is then cancelled based on the least squares method, and the steps are repeated for the next most significant component, until all significant components are identified. The iterative algorithm is terminated by using the threshold,

$$\mathrm{Th}(\mathbf{Z}_m^{(\mathrm{o})}) = 2S\left(\mathbf{Z}_m^{(\mathrm{o})}\right) = \frac{1}{N}\sum_{k=0}^{N-1}\left|\sum_{n=0}^{N-1}\mathbf{Z}_m^{(\mathrm{o})}(n)e^{-j2\pi\frac{kn}{N}}\right|, \tag{51}$$

where $S\left(\mathbf{Z}_m^{(\mathrm{o})}\right)$ is the average spectrum of $\mathbf{Z}_m^{(\mathrm{o})}$ (the spectrum of noise of $\mathbf{Z}_m^{(\mathrm{o})}$ will be below $\mathrm{Th}(\mathbf{Z}_m^{(\mathrm{o})})$, and "o" denotes "p" or "s". The termination condition is set as,

$$\left|\sum_{n=0}^{N-1}\left(\mathbf{Z}_m^{(\mathrm{o})}\right)^{(l)}(n)e^{-j2\pi\frac{nf_k}{f_s}}\right| \leq \mathrm{Th}(\mathbf{Z}_m^{(\mathrm{o})}), \quad \text{for } \forall f_k \tag{52}$$

where l is the final number of selected f_{mi}. This condition ensures that all the significant interference components (outside the NQR band) whose spectrum is above the noise level will be cancelled by the IC method.

Table 1: Steps for the IC method outside the NQR band [12]

["o" denotes "p" or "s"; $m = 1, 2, ..., M$.]

i=0;

$\left(\mathbf{Z}_m^{(\mathrm{o})}\right)^{(0)}$=$\mathbf{Z}_m^{(\mathrm{o})}$;

while $\left(\exists f_k, \left|\sum_{n=0}^{N-1}\left(\mathbf{Z}_m^{(\mathrm{o})}\right)^{(i)}(n)e^{-j2\pi\frac{nf_k}{f_s}}\right| > \mathrm{Th}(\mathbf{Z}_m^{(\mathrm{o})})\right)$

i=i+1;

$f_{mi} = \arg\min_{f_k} C\left(f_k, \left(\mathbf{Z}_m^{(\mathrm{o})}\right)^{(i-1)}\right)$

$=\arg\min_{f_k}\left[\left\|\left(\mathbf{Z}_m^{(\mathrm{o})}\right)^{(i-1)} - \mathbf{F}(f_k)\mathbf{F}^{\dagger}(f_k)\left(\mathbf{Z}_m^{(\mathrm{o})}\right)^{(i-1)}\right\|_2^2\right]$;

$\left(\mathbf{Z}_m^{(\mathrm{o})}\right)^{(i)} = \mathbf{Z}_m^{(\mathrm{o})}$

$-[\mathbf{F}(f_{m1}) \quad ... \quad \mathbf{F}(f_{mi})][\mathbf{F}(f_{m1}) \quad ... \quad \mathbf{F}(f_{mi})]^{\dagger}\mathbf{Z}_m^{(\mathrm{o})}$;

end

This algorithm can cancel interference outside the NQR band accurately with very little distortion of the NQR signal [12]. As interference frequencies at the two antenna are the same, the estimated frequency values at one channel can be used by the other thus saving the calculation cost of an iteration. However, the merit of doing estimation for the two channels separately is that associating the two estimation results may increase the confidence level of the estimation, as well as alarm the possible hardware fault if there is big difference between the two group of estimated frequencies.

We note that there are situations where combining the IC method can be challenging, as the interference centered inside the NQR band may have sidelobes located outside the NQR band (see Fig.9 for example). If a sidelobe exceeds the threshold set in Eq.(51), it will be cancelled in the IC process (see Table 1), resulting in a significant distortion of the interference centered inside the NQR band, which will have an adverse effect in the subsequent application of the BIC method. To overcome this problem, we can first apply the IC process to the whole frequency band $\left[-\frac{f_s}{2}, \frac{f_s}{2}\right]$. Referring to Table 1, we note the frequencies of all the acquired significant components are $[f_{m1}, f_{m2}, ..., f_{ml}]$. The corresponding estimated amplitudes of them should be

$$[\beta_{m1} \quad \beta_{m2} \quad ... \quad \beta_{ml}]^{\mathrm{T}} = [\mathbf{F}(f_{m1}) \quad \mathbf{F}(f_{m2}) \quad ... \quad \mathbf{F}(f_{ml})]^{\dagger}\mathbf{Z}_m^{(\mathrm{o})}. \tag{53}$$

From the congregation $[f_{m1}, f_{m2}, ..., f_{ml}]$, we select all the frequencies $[f_{ml_1}, f_{ml_2}, ..., f_{ml_l}]$ that are

outside the NQR band, where $1 \leq l_1, l_2, ..., l_l \leq l$. Then we can cancel the interference outside the NQR band causing little distortion to the NQR signal and the interference inside the NQR band as

$$\begin{aligned}\left(\mathbf{Z}_m^{(\mathrm{o})}\right)^{(l_l)} = \mathbf{Z}_m^{(\mathrm{o})} - [\mathbf{F}(f_{ml_1}) \quad \mathbf{F}(f_{ml_2}) \quad ... \quad \mathbf{F}(f_{ml_l})] \\ \cdot [\beta_{ml_1} \quad \beta_{ml_2} \quad ... \quad \beta_{ml_l}]^{\mathrm{T}}.\end{aligned} \tag{54}$$

To summarize the steps of our approach, we can write a workflow for the BICETAML algorithm as:

"Cancel interference outside NQR band to get $\left(\mathbf{Z}_m^{(\mathrm{p})}\right)^{(l_l)}$ and $\left(\mathbf{Z}_m^{(\mathrm{s})}\right)^{(l_l)}$" → "use BIC method on $\left(\mathbf{Z}_m^{(\mathrm{p})}\right)^{(l_l)}$ and $\left(\mathbf{Z}_m^{(\mathrm{s})}\right)^{(l_l)}$ to get $\left(\mathbf{Z}_m^{(\mathrm{p})}\right)_c^{(l_l)}$=$\left(\mathbf{Z}_m^{(\mathrm{p})}\right)^{(l_l)} - \hat{\sigma}_c e^{j2\pi\hat{f}_c \mathbf{t}}\hat{\phi}_m$" → "apply ETAML algorithm to $\left(\mathbf{Z}_m^{(\mathrm{p})}\right)_c^{(l_l)}$".

III. THE PERFORMANCE OF THE BICETAML ALGORITHM

This section presents results from simulated and experimental data to assess the performance of the BICETAML algorithm and its combination with a prior step of IC method to cancel interference outside the NQR band. The simulated data was created to resemble the experimental data of interest, which involves detection of sodium nitrite in laboratory conditions (see Section III-D for details).

We compare the BICETAML results to results of applying the previously proposed algorithms ETAML and FETAML [8]. Besides, the results by the beamforming detectors based on the current discussed TE data acquisition system, Eq.(20), Eq.(27), and Eq.(33) termed TEBFD_Capon, TEBFD_ML, and TEBFD_MLf respectively, are also within the following discussion.

A. Simulation I: Single frequency interference within the NQR band

We first simulated a TE data-set consisting of 1000 Monte Carlo runs, where each run has M=10 echoes and each echo comprises of N=128 data points. The parameters of the NQR signal are set to be $\check{f}$=$2f_s/N$, where f_s=$\frac{1}{16}$MHz, $|\alpha|$=0.2, T^*=1.7ms, and T^e=2s, respectively. The NQR band is assumed to be $[f_s/N, 3f_s/N]$, and the noise is assumed white Gaussian with variance $\sigma^2_{N\mathrm{p}}$=0.125 and $\sigma^2_{N\mathrm{s}}$=6.125. The signal to noise ratio (SNR) can be calculated as,

$$\mathrm{SNR} = 20\lg\left(\frac{\pi}{4} \cdot \frac{|\alpha|^2}{\sigma^2_{N\mathrm{p}}}\right), \tag{55}$$

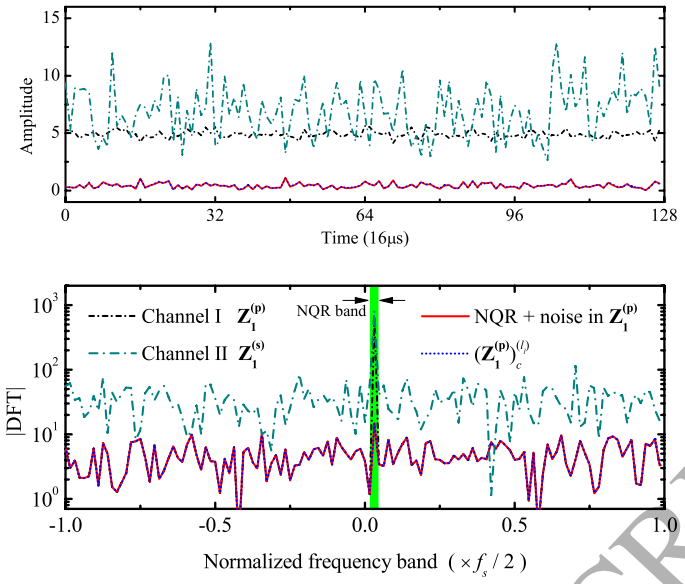

FIG. 2. (Color online) $\mathbf{Z}_1^{(p)}$ from a Monte Carlo run of the N=128 simulated data (containing a single frequency interference within the NQR band) and its interference cancelled result in the time and frequency domains. "|DFT(·)|" means the absolute value of Discrete Fourier transformation of data. The vertical axis of frequency domain is base-10 logarithmic.

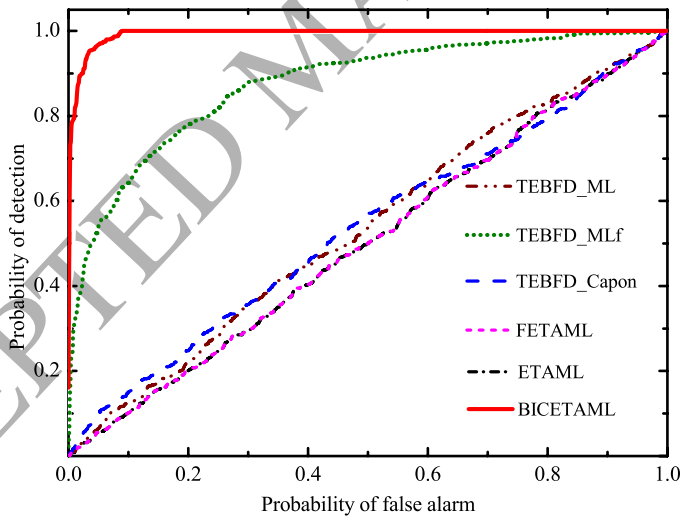

FIG. 3. (Color online) The ROC curves obtained by ETAML, FETAML, TEBFDs, and BICETAML algorithms for the N=128 simulated data containing a single frequency interference within the NQR band.

and is about -12dB. We set these parameters by referring to our experiments. The search ranges of T^* and T^e, by referring to the NQR theory [20] and our laboratory conditions, can be set as [1.7/2, 1.7*2]ms and [1, 3]s, respectively. Please note that $\sigma_{Ns}^2 \gg \sigma_{Np}^2$ is set in order to simulate

a challenging NQR detection task. In fact in our experiments, the secondary channel's probe exposed thoroughly in the background environment is more likely to receive stronger noise or interference compared to the primary channel's which is adjusted to focus on receiving NQR signals (see Fig.9). We added strong interference to the data within the NQR band. Its frequency is the same as the NQR signal's. σ_c is set to be 5. We also considered amplitude and phase differences of interference between the two channels, in particular, ϵ=0.25 and $\Delta\varphi=\pi/3$ in Eq.(14).

Figure 2 shows the interference cancellation results for $\mathbf{Z}_1^{(\mathrm{p})}$ from a Monte Carlo run. It is clear that although the interference almost coincides with the NQR signal, BICETAML algorithm can cancel it precisely without distorting the NQR signal or noise as $\left(\mathbf{Z}_1^{(\mathrm{p})}\right)_c^{(l_l)}$ is very similar to the "NQR + noise in $\mathbf{Z}_1^{(\mathrm{p})}$". As a result, the receiver operating characteristic (ROC) curves in Fig.3 shows a good performance of BICETAML. The ETAML and FETAML algorithms, on the other hand, exhibit very bad performance in this case. Although Eq.(7), Eq.(31), and "$\bar{\mathbf{x}}\rightarrow[\alpha P_s \quad 0]^{\mathrm{T}}$ for large enough M" suggest that ETAML would be able to make a valid detection based on the TE data acquisition system, the calculation result indicates that the convergence from $\bar{\mathbf{x}}(1)$ to αP_s goes slowly with the increment of M. In other words, ETAML (as well as FETAML) fails to handle the interference in this case. The performances of TEBFD_Capon and TEBFD_ML are also bad. Since that here $\overline{\sigma^2(t)}\simeq|\alpha|^2=0.04\ll\sigma_{N\mathrm{p}}^2+\frac{\sigma_c^2\sigma_{N\mathrm{s}}^2}{(1+\epsilon)^2\sigma_c^2+\sigma_{N\mathrm{s}}^2}$, NQR signal information in Capon beamforming output (see Eq.(20)) is severely masked by the strong noise and interference. In fact, the TEBFD_ML has good performance if only $\sigma_{N\mathrm{s}}^2$ (Channel II) is not very large, according to our further numerical tests. It is noted that the performance of TEBFD_MLf is not bad, though it can not match that of the proposed BICETAML algorithm, since all the strong noise, in Channel II and outside the NQR band, is effectively "cancelled" by the frequency selective method in TEBFD_MLf. The proposed BIC method is robust to the strong noise of Channel II according to Eqs.(39) and (41), and the subsequent ETAML is only applied to data of Channel I.

1. robustness analysis on BIC

As mentioned before, the spectrometer's full relaxation time is too short for parameters to change significantly in many practical applications. However, it is necessary to check if the proposed BIC method degrades with parameters' variation with time. To do this, we let the four key parameters $\{\sigma_c, f_c, \epsilon, \Delta\varphi_c\}$ in BIC vary randomly among the echoes, that is, in each echo, they are $\{\sigma_c, f_c, \epsilon, \Delta\varphi_c\}+v\cdot\mathrm{random}\,\{[\pm r_1, \pm r_2, \pm r_3, \pm r_4]\}$, where random($\pm r_i$) ($r_i$>0) means a random value

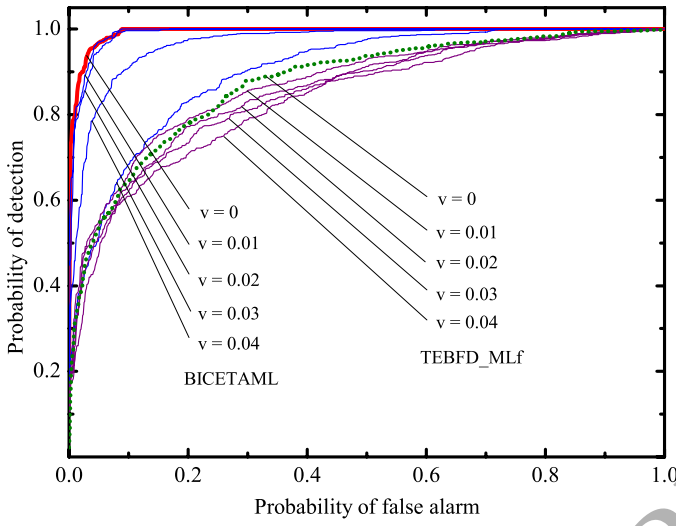

FIG. 4. (Color online) The ROC curves obtained by BICETAML and TEBFD_MLf at different scales (v) of parameters' variation, as a robustness comparison between BICETAML and TEBFD_MLf.

picked within the interval $[-r_i, r_i]$ and v is a scale of parameters' variation. This is introduced to the above mentioned simulated TE data-set. In specific, we let $r_1=\sigma_c$, $r_2=f_s/N$, $r_3=1$, and v = 0.01, 0.02, 0.03, 0.04. Besides, we let $\Delta\varphi_c$ be $2\pi\left[f_c + v\cdot\text{random}(\pm f_s/N)\right]\cdot\left[\frac{1}{6f_c} + v\cdot\text{random}(\pm\frac{1}{6f_c})\right]$ (which is the original $\Delta\varphi_c=\pi/3$ when v=0), considering that the variation of $\Delta\varphi_c$ is affected both by the changes of interference frequency f_c and the time difference between the two channels. Figure 4 shows the robustness comparison between BICETAML and TEBFD_MLf. BICETAML has better performance on this data-set but indeed worse robustness compared to TEBFD_MLf. For BICETAML, we need not to specially consider the variation of NQR parameters $\left[\check{f} \quad T^* \quad T^e\right]$ because the NQR signal is weak compared to the interference and NQR parameters' variation has little influence on BIC's performance. Besides, the subsequent ETAML is robust to the variation of $\left[\hat{\check{f}} \quad \hat{T}^* \quad \hat{T}^e\right]$ according to our tests.

2. A 64-points-per-echo (N=64) simulated TE data-set

Humanitarian demining and security checking may demand a shorter time of data acquisition which leads to fewer sampling points per echo. We present another simulation with N=64 in order to check if the proposed method's performance suffers degradation due to the points reduction. This new N=64 TE data-set inherits parameters from the present N=128 one. However, we let $\check{f}$=$-0.3f_s/N$ with the corresponding NQR band being $[-1.3f_s/N, 0.7f_s/N]$ and $f_c = -0.4f_s/N$ by

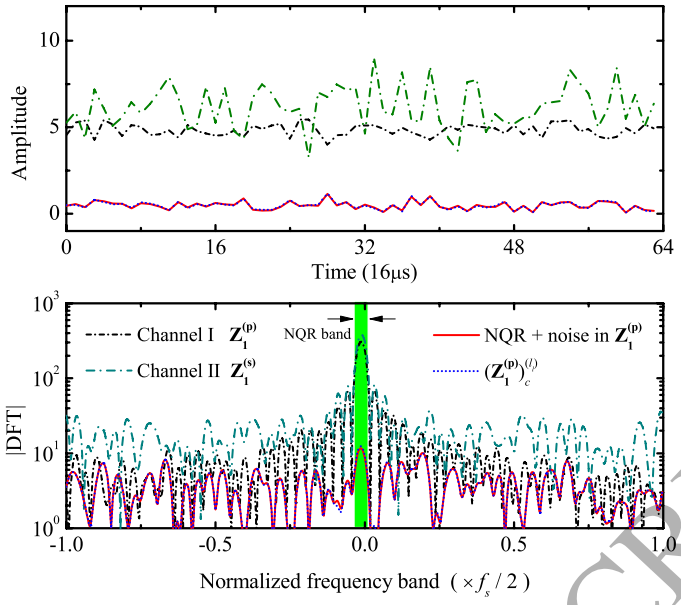

FIG. 5. (Color online) $\mathbf{Z}_1^{(p)}$ from a Monte Carlo run of the N=64 simulated data (containing a single frequency interference within the NQR band) and its interference cancelled result in the time and frequency domains. "|DFT(·)|" means the absolute value of Discrete Fourier transformation of data. The vertical axis of frequency domain is base-10 logarithmic.

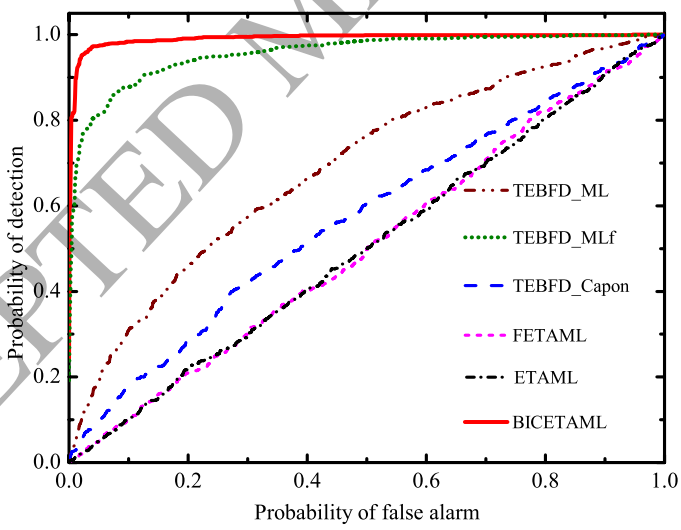

FIG. 6. (Color online) The ROC curves obtained by ETAML, FETAML, TEBFDs, and BICETAML algorithms for the N=64 simulated data containing a single frequency interference within the NQR band.

referring to our experimental data (see Section III-C). Besides, the noise intensity at Channel II is lowered to be 2. As we can see in Figs.5 and 6, BICETAML still performs well in interference

cancellation and the final NQR detection for this N=64 data-set. Please note that the frequency domain information is presented at the lower row of Fig.5 by using zero-padding FFT, as the regular 64 points FFT provides unsatisfied frequency resolution. By padding 640-64=576 zero points following the end of the 64-points echo (see Fig.5), the effective minimal frequency resolution becomes $f_s/N/10$ (about 100Hz).

B. Simulation II: Additional interference of multiple frequencies outside the NQR band

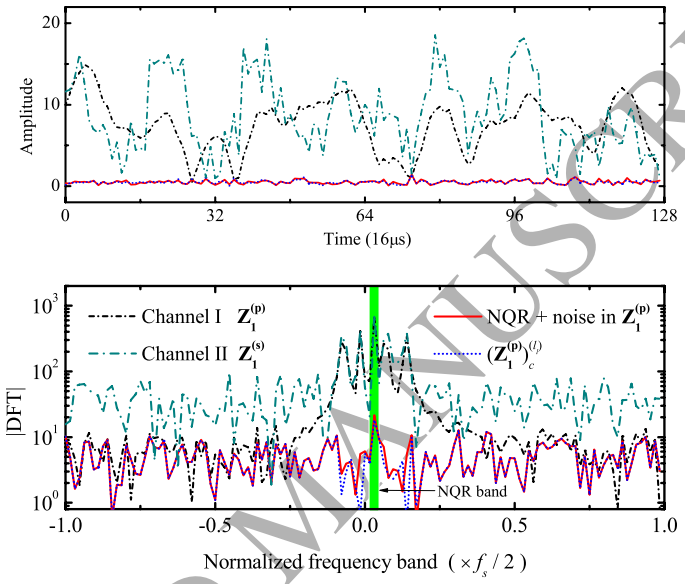

FIG. 7. (Color online) $\mathbf{Z}_1^{(p)}$ from a Monte Carlo run of the N=128 simulated data (containing interference of multiple frequencies outside the NQR band in addition to the interference of Section III-A) and its interference cancelled form in the time and frequency domains. "|DFT(·)|" means the absolute value of Discrete Fourier transformation of data. The vertical axis of frequency domain is base-10 logarithmic.

Interference for this case was produced by adding multiple frequency components outside the NQR band to the TE data-set (the N=128 one) of Section III-A. Their frequencies are not far from the NQR band, resulting in strong overlaps between the component centered inside the NQR band and themselves. Similar to the case of Section III-A, we have included amplitude and phase differences between the two channels for the interference components outside the NQR band. Please note that calibration error may vary among different frequency components as mentioned before. For simplicity but without loss of generality, we set the amplitudes of all the interference frequency components outside the NQR band to be 3 at Channel I and 4 at Channel II, respectively.

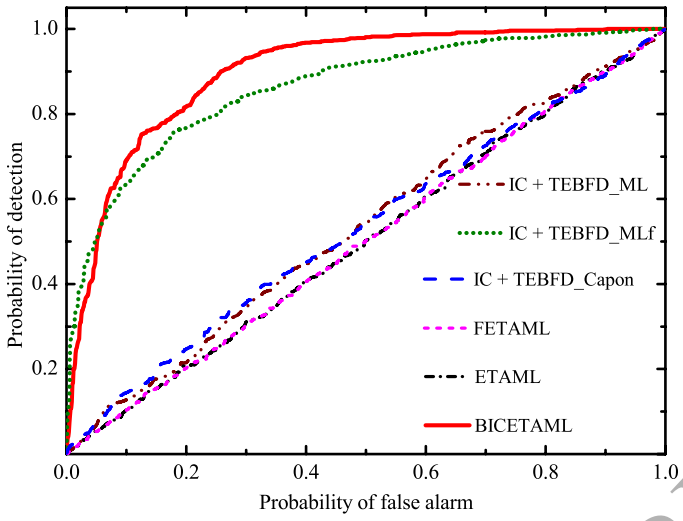

FIG. 8. (Color online) The ROC curves obtained by ETAML, FETAML, TEBFDs, and BICETAML algorithms for the N=128 simulated data containing interference of a frequency inside and multiple frequencies outside the NQR band.

As discussed in Section II-F, this case requires cancelling the significant interference components outside the NQR band (without distorting the component inside the NQR band) prior to applying BICETAML. This interference cancellation (IC) is also the pretreatment of applying the TEBFDs. The result of BIC is displayed in Fig.7 which shows that all the significant interference components are removed effectively and the NQR signal peak in the frequency domain is restored nicely after the BIC process. However, in contrast to the case of Section III-A, the residual interference in this case inevitably causes a slight performance degradation on BICETAML (see the ROC curves in Figs. 3 and 8). The other algorithms, except for IC + TEBFD_MLf, exhibit bad performance in this case. It is noted that although BICETAML has better performance, TEBFD_MLf suffers much less performance degradation from the multiple frequency components outside the NQR band than BICETAML.

C. Experimental data test

We present here results from measured data, collected in an laboratory experiment where our aim was to detect the ^{14}N NQR signal due to sodium nitrite ($NaNO_2$), suspended in silicone oil sealed in a plastic box buried under soil. We also performed the same measurement without $NaNO_2$ to examine false alarms of the BICETAML algorithm. The data signal comprises

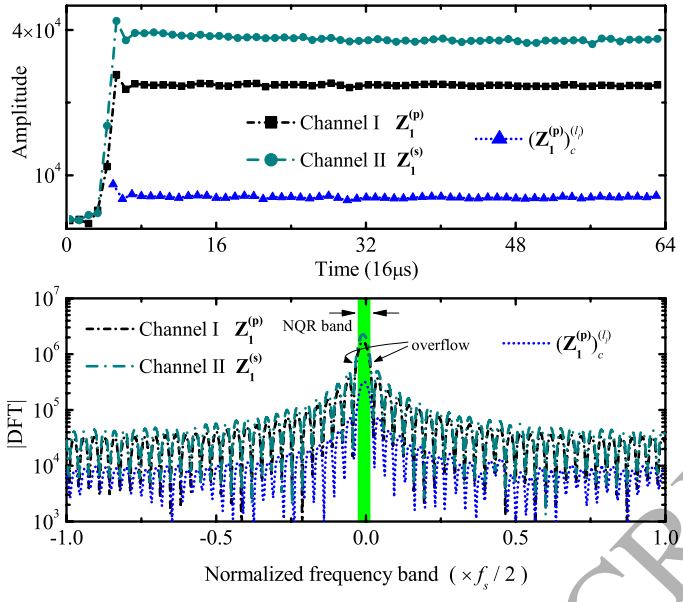

FIG. 9. (Color online) $\mathbf{Z}_1^{(p)}$ from a run of the experimental data and its interference cancelled form in the time and frequency domains. "|DFT(·)|" means the absolute value of Discrete Fourier transformation of data. The vertical axis of frequency domain is base-10 logarithmic.

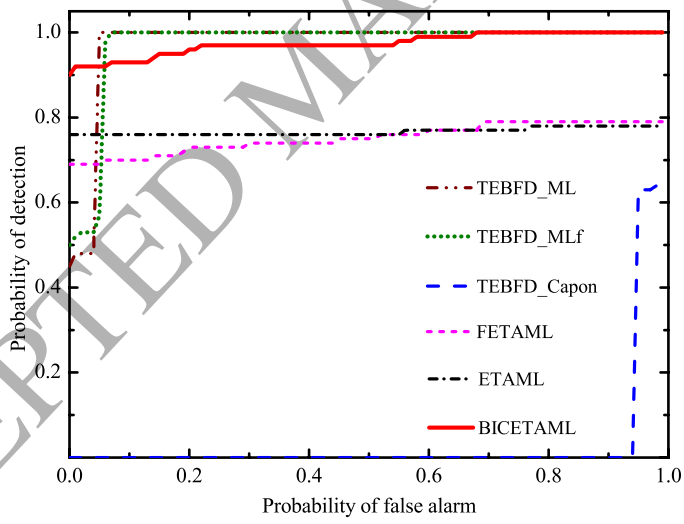

FIG. 10. (Color online) The ROC curves obtained by ETAML, FETAML, TEBFDs, and BICETAML algorithms for the experimental data.

of M=10 echoes with each echo including N=64 sampling points with a sampling frequency f_s being $\frac{1}{16\mu s}$. Under our laboratory conditions and NQR theory predictions [20], the NQR signal has a resonant frequency $\check{f}\simeq$3.5997MHz with b=600Hz/Kelvin in Eq. (9), and its parameters T^*

and T^e in Eq. (1) satisfy $T^*\simeq$1.7ms, and $T^e\simeq$2s, respectively. The frequency band $\left[-\frac{f_s}{2}, \frac{f_s}{2}\right]$ of the recorded data is modulated from the exact frequency band $\left[f_o - \frac{f_s}{2}, f_o + \frac{f_s}{2}\right]$ of the received signal, where f_o=3.6MHz denotes the frequency center of modulation. Thus, the effective NQR frequency is about $\check{f}$-f_o=-0.3kHz. Since our lab temperature uncertainty ΔT during experiments is about 1.7Kelvin, the effective NQR band is about $[-1.3\text{kHz}, 0.7\text{kHz}]$ according to Eq. (10).

We acquired an experimental data-set consisting of 100 runs. The frequency of the recorded interference is within the NQR band and very close to the exact NQR frequency. Figure 9 shows a run of the experimental data in both time and frequency domains. Compared to the aforementioned N=64 simulated data, the signal to noise and to interference ratios are relatively larger. However, by pre-scanning the experimental data, we found that random uncertainties/defects inevitably occur during our measurements, which challenges the usability of the proposed BICETAML algorithm. Moreover, our TE system has a recovery time between any two neighbor echoes, resulting in 5 invalid points at the beginning of each echo (see the upper row of Fig.9). We need to "discard" these 5 points by setting the first 5 points of $\mathbf{Z}_{NM}$, $\mathbf{Q}_{NM}$, $\mathbf{Z}_m^{(\mathrm{p})}$, and $\mathbf{Z}_m^{(\mathrm{s})}$ to be zero, and by considering only the 6th - 64th points of $\mathbf{t}$, $\mathbf{Z}_m^{(\mathrm{p})}$, and $\mathbf{Z}_m^{(\mathrm{s})}$ in Eqs.(43) to (49). Like in Fig.5, zero-padding FFT is also used in Fig.9 for a better frequency resolution. Due to discarding the 5 invalid points, the exact number of zero points padded at the end of each echo is 640-64+5=581.

The interference cancellation result and ROC curves are show in Figs.9 and 10, respectively. The figures confirm that the BICETAML algorithm is effective for cancelling interference within the NQR band, leading to efficient NQR detection, as opposed to ETAML, FETAML and TEBFD_Capon algorithms. The TEBFD_ML and TEBFD_MLf algorithms constructed on the TE system also exhibit good performance at this experimental case. However, BICETAML is slightly better than them, as the area below the BICETAML's ROC curve is slightly larger than that below TEBFD_ML's or TEBFD_MLf's ROC curve.

IV. CONCLUSION

This paper presents a novel algorithm based on a two-channel echo-train (TE) data acquisition system for NQR signal detection. The algorithm contains an advanced beamforming approach which complements our previous IC method [12] by dealing with interference which is centered inside the NQR band. Coupled with our previous work [12] on interference cancellation, the proposed BICETAML algorithm can also cancel interference outside the NQR band (i.e. within the

whole signal spectrum). After interference cancellation, the proposed algorithm uses the previously developed ETAML algorithm to perform NQR detection. Our preliminary simulation and experimental results suggest BICETAML's potential to detect NQR signals contaminated by interference in real-life settings. The results show that BICETAML outperforms the previously proposed ETAML and FETAML algorithms as well as the classical beamforming detectors constructed on the TE system. This proposed BICETAML algorithm has considered that the interference inside the NQR band is single-frequency, which is reasonable as the NQR band is usually very narrow and the possible sources of the strong interference are usually the electric appliances which are almost single-frequency. Our future work will deal with multiple-frequency interference within a single NQR band, and/or with NQR signals with more than one NQR bands (i.e. resonant frequencies).

V. APPENDIX

Once $\overline{\overline{\mathbb{R}}}$ is acquired, one may also consider estimating the absolute interference amplitude σ_c based on RCB [13] method. The RCB estimation problem is described as,

$$\begin{aligned} &\min_{\mathbf{a}_{\mathrm{RCB}}} \mathbf{a}_{\mathrm{RCB}}{}^{\mathrm{H}} \left(\overline{\overline{\mathbb{R}}}\right)^{-1} \mathbf{a}_{\mathrm{RCB}} \quad \text{subject to } \|\mathbf{a}_{\mathrm{RCB}} - \bar{\mathbf{a}}_c\|^2 \le \bar{\epsilon}^2, \\ &\hat{\sigma}_c = \sqrt{\mathrm{BO\_RCB}} = \sqrt{\frac{1}{\left|\mathbf{a}_{\mathrm{RCB}}{}^{\mathrm{H}} \left(\overline{\overline{\mathbb{R}}}\right)^{-1} \mathbf{a}_{\mathrm{RCB}}\right|}}, \end{aligned} \tag{56}$$

where $\bar{\mathbf{a}}_c = \left[1 \quad e^{j\Delta\bar{\varphi}_c}\right]^{\mathrm{T}}$, and $\Delta\bar{\varphi}_c$ and $\bar{\epsilon}$ are the prior knowledge of $\Delta\varphi_c$ and ϵ, respectively. One can solve the RCB problem deriving the expression of BO_RCB as a function of $\Delta\bar{\varphi}_c$ and $\bar{\epsilon}$. For investigating the performance of RCB, we select a Monte Carlo run of the N=128 simulated data mentioned in Section III-A as an example. As $\Delta\bar{\varphi}_c$ and $\bar{\epsilon}$ are unknown in the present problem, we replace $\Delta\bar{\varphi}_c$ and $\bar{\epsilon}$ in the expression of BO_RCB with Δ_y and ϵ_x respectively and name the new expression as BO_RCBf, and plot the calculated $\sqrt{\mathrm{BO\_RCB}f}$, based on the example, as a function of Δ_y and ϵ_x in Fig.11. As we can see, $\hat{\sigma}_c$ is about 6.66 when $\Delta\varphi_c$ and ϵ are exactly known (Δ_y=$\pi/3$ and ϵ_x=0.25), which is not precise enough as the true value of σ_c is 5. Besides, $\sqrt{\mathrm{BO\_RCB}f}$ does not have an extremum, which prohibits the searching method as shown in Eq.(42) from addressing an estimation for σ_c.

On the contrary, as shown in Fig. 12, $\hat{\sigma}_c$ given by the proposed BIC method is very closed to 5 according to Eq.(42). The values of ϵ_x and Δ_y corresponding to $\hat{\sigma}_c$ are also consistent with ϵ and

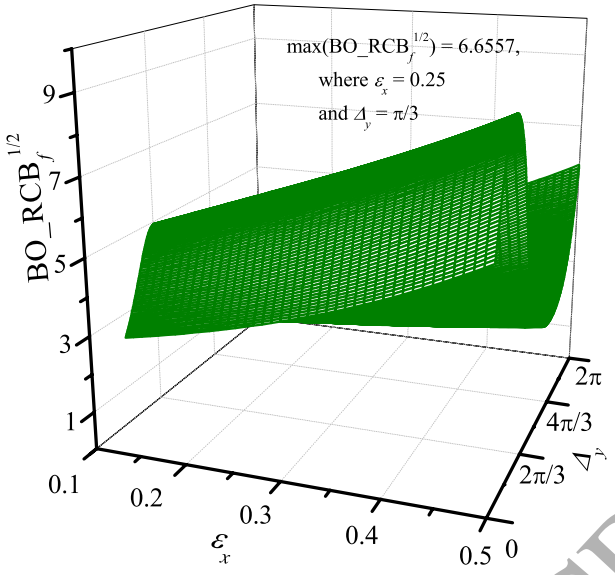

FIG. 11. (Color online) The $\sqrt{\text{BO\_RCB}f}$, as a function of Δ_y and ϵ_x, for a Monte Carlo run of the N=128 simulated data in Section III-A.

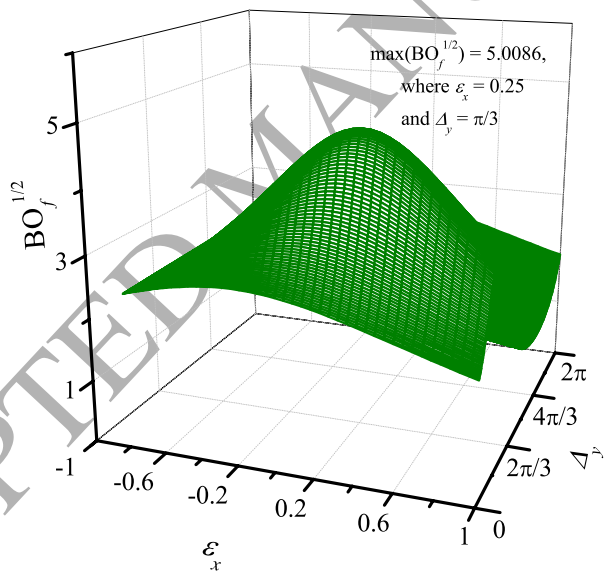

FIG. 12. (Color online) The $\sqrt{\text{BO}_f}$, as a function of ϵ_x and Δ_y, for a Monte Carlo run of the N=128 simulated data in Section III-A.

$\Delta\varphi_c$, respectively.

ACKNOWLEDGMENT

This work has been supported by Find a Better Way (FABW) UK, under Project AQUAREOS.

REFERENCES

[1] J. A. S. Smith, "Nuclear quadrupole resonance spectroscopy," *J. Chem. Educ.*, vol. 48, no. 1, pp. 39–48, 1971.

[2] N. R. Butt, E. Gudmundson, and A. Jakobsson, "An overview of NQR signal detection algorithms," in *Magnetic Resonance Detection of Explosives and Illicit Materials*, ser. NATO Science for Peace and Security Series B: Physics and Biophysics, T. Apih, B. Rameev, G. Mozzhukhin, and J. Barras, Eds. Springer, 2013, pp. 19–34.

[3] J. Barras, D. Murnane, K. Althoefer, S. Assi, M. D. Rowe, I. Poplett, G. Kyriakidou, and J. A. S. Smith, "Nitrogen-14 nuclear quadrupole resonance spectroscopy: a promising new analytical methodology for medicines authentication and counterfeit antimalarial analysis," *Anal. Chem.*, vol. 84, pp. 2746–2753, 2013.

[4] J. Barras, K. Althoefer, M. D. Rowe, I. Poplett, and J. A. S. Smith, "The emerging field of nuclear qudrupole resonance-based medicines authentication," *Appl. Magn. Reson.*, vol. 43, pp. 511–529, 2012.

[5] M. D. Rowe and J. A. S. Smith, "Mine detection by nuclear quadrupole resonance," *in Proc. EUREL Int. Conf. on the Detection of Abandoned Land Mines*, pp. 62–66, Oct. 1996.

[6] A. Gregorovič and T. Apih, "Relaxation during spin-lock spin-echo pulse sequence in n 14 nuclear quadrupole resonance," *J. Chem. Phys.*, vol. 129, p. 214504, 2008.

[7] A. Jakobsson, M. Mossberg, M. D. Rowe, and J. A. S. Smith, "Exploiting temperature dependency in the detection of nqr signals," *IEEE Trans. Signal Proces.*, vol. 54, no. 5, pp. 1610–1616, 2006.

[8] S. D. Somasundaram, A. Jakobsson, J. A. S. Smith, and K. Althoefer, "Exploiting spin echo decay in the detection of nuclear quadrupole resonance signals," *IEEE Trans. Geosc. Remote Sensing*, vol. 45, pp. 925–933, 2007.

[9] Y. Tan, S. L. Tantum, and L. M. Collins, "Cramerrao lower bound for estimating quadrupole resonance signals in non-gaussian noise," *IEEE Signal Process. Lett.*, vol. 11, no. 5, pp. 490–493, 2004.

[10] W. Shao, J. Barras, and P. Kosmas, "Detection of extremely weak nqr signals using stochastic resonance and neural network theories," *Signal Processing*, vol. 142, pp. 96–103, 2018.

[11] A. Jakobsson, M. Mossberg, M. D. Rowe, and J. A. S. Smith, "Frequency-selective detection of nuclear quadrupole resonance signals," *IEEE Trans. Geosc. Remote Sensing*, vol. 43, no. 11, pp. 2659–2665, 2005.

[12] W. Shao, J. Barras, K. Althoefer, and P. Kosmas, "Detecting nqr signals severely polluted by interference," *Signal Processing*, vol. 138, pp. 256–264, 2017.

[13] J. Li, P. Stoica, and W. Wang, "On robust capon beamforming and diagonal loading," *IEEE Trans. Signal Proces.*, vol. 51, no. 7, pp. 1702–1715, 2003.

[14] P. Stoica, H. Xiong, L. Xu, and J. Li, "Adaptive beamforming for quadrupole resonance," *Digital Signal Processing*, vol. 17, pp. 634–651, 2007.

[15] N. R. Butt and A. Jakobsson, "Robust multi-sensor detection of polymorphic nqr signals," *2007 Conference Record of the Forty-First Asilomar Conference on Signals, Systems and Computers*.

[16] A. Jakobsson and M. Mossberg, "Using spatial diversity to detect narcotics and explosives using nqr signals," *IEEE Trans. Signal Proces.*, vol. 55, no. 9, pp. 4721–4726, 2007.

[17] Y. Jiang, P. Stoica, and J. Li, "Array signal processing in the known waveform and steering vector case," *IEEE Trans. Signal Proces.*, vol. 52, no. 1, pp. 23–35, 2004.

[18] T. Piatti, S. Lei, J. Barras, and A. Jakobsson, "Interference cancellation in two-channel nuclear quadrupole resonance measurements," *Icassp, 2017*.

[19] N. R. Butt and A. Jakobsson, "Efficient removal of noise and interference in multichannel quadrupole resonance," *in Proceedings of the 45th Asilomar Conference*, pp. 1072–1076, 2011.

[20] S. D. Somasundaram, "Advanced signal processing algorithms based on novel nuclear quadrupole resonance models for the detection of explosives," Ph.D. dissertation, King's College London, 2007.

[21] S. M. Kay, *Fundamentals of Statistical Signal Processing, Volume II: Detection Theory*. Englewood Cliffs, NJ: Prentice-Hall, 1998.

[22] P. Stoica and R. L. Moses, *Introduction to Spectral Analysis*. Englewood Cliffs, NJ: Prentice-Hall, 1997.